

中国激光

基于单共振光学参量振荡器实现近红外到中红外激光输出的实验研究

王海龙¹, 杨慧琦¹, 苏静^{1,2}, 卢华东^{1,2*}

¹ 山西大学光电研究所量子光学与光量子器件国家重点实验室, 山西 太原 030006;

² 山西大学极端光学协同创新中心, 山西 太原 030006

摘要 利用结构紧凑的四镜环形单共振光学参量振荡器(SRO)实现了从近红外到中红外的瓦级单频激光输出。通过优化谐振腔腔镜的曲率半径以及谐振腔腔长,设计了双腰斑的四镜环形谐振腔,在两个腰斑处分别放置光学参量振荡晶体 MgO:PPLN 和倍频晶体 PPKTP。当单频 1064 nm 泵浦激光的注入功率为 21 W 时,得到了 2.1 W 的 1550 nm 信号光、1.1 W 的 775 nm 倍频光以及 1.7 W 的 3393 nm 闲频激光输出,总光光转换效率为 23.3%,5 h 内信号光、倍频光、闲频光的功率稳定性(均方根)分别优于 2.5%、1.6%、0.8%。本团队研制的单频连续波激光器可以应用于包括压缩态光场和纠缠态光场等非经典光场制备的实验中。

关键词 激光; 单共振光学参量振荡器; 倍频; 四镜环形腔; 单频; 热透镜效应

中图分类号 TN248.1

文献标志码 A

DOI: 10.3788/CJL202249.1801005

1 引言

全固态连续波单频激光器以其结构紧凑、噪声低和光束质量好等优点被广泛应用于科研、军事、医疗、工业等领域。但是由于受到激光晶体自身荧光光谱的限制,激光的发射波长只能限制在特定的范围内,不能满足快速发展的科学研究需要。包括光参量振荡(OPO)、和频、差频等在内的非线性频率变换作为一种有效的激光波长变换技术,可以将激光波长变换到深紫外和中红外区域,甚至是远红外区域^[1-2],有效拓展了激光器的输出波长范围,满足了不同领域的应用需求^[3-4]。

在量子精密测量和量子通信等量子研究中,为保证激光在光纤中远距离传输,激光光源一般使用的是位于光纤低损耗和低色散窗口的 1550 nm 激光。目前产生 1550 nm 激光的方法主要有三种:1)由 976 nm 半导体激光器泵浦钕共掺晶体直接产生,这种方法具有成本低廉、结构紧凑等优点。尽管钕共掺晶体存在固有的激发态吸收和吸收损耗等问题,但在 2021 年,山西大学的张宽收研究小组利用蓝宝石-Er, Yb:YAB-蓝宝石的三明治结构,结合双端面偏振抽运耦合系统,提高了钕共掺晶体端面的散热效率并降低了晶体的热沉积,在抽运功率为 11.7 W 时实现

了 755 mW 的单频连续波 1.5 μm 激光输出,这是目前钕共掺晶体单频连续输出 1.5 μm 激光的最高指标^[5]。2)由掺铒光纤激光器产生。由于激光器为波导式结构,因此光纤内可以产生较高的功率密度,容易实现大功率激光输出。目前 Nuphoton 公司研制的商品化 1.5 μm 连续波单纵模光纤激光器的输出功率可达 5 W 以上,但其输出激光的噪声也较大,若要进行量子实验,需要使用模清洁剂^[6]或者马赫-曾德尔干涉仪^[7]等器件来降低激光器的强度噪声。3)OPO 技术。相比于前两种方法,OPO 技术同时兼具低噪声、窄线宽和高稳定性等优点^[8],越来越受到量子光学实验和量子信息研究等领域的重视,并且非线性晶体制作技术的不断成熟,尤其是周期极化非线性晶体的快速发展,为实现高质量单频连续波激光输出提供了保障^[9]。

在多组分纠缠态制备时,不仅要用高功率的单频连续波 1.5 μm 激光器作为多个 OPO 的种子源,而且后续还要用以种子源的倍频光作为光学参量放大器(OPA)的泵浦光来产生非经典压缩态光场^[10]。目前,在量子光源的产生中,1550 nm 激光及其倍频光一般是使用两个分立的腔来实现的,但是,过多的谐振腔会增大实验装置的体积以及腔模耦合的难度。基于此,本团队希望将光参量振荡过程和二次谐波产生(SHG)过程放入同一个腔内来实现 1550 nm 及其倍

收稿日期: 2022-01-05; 修回日期: 2022-01-23; 录用日期: 2022-01-25

基金项目: 国家自然科学基金(61975100, 62027821, 62105192)、山西省 1331 工程项目、山西省高等学校中青年拔尖创新人才支持计划

通信作者: *luhuadong@sxu.edu.cn

频光的双波长输出,所以在设计腔时就需要有两个小的激光腰斑。Shukla等^[11]和Devi等^[12]都利用六镜环形腔结构来实现腔内双腰斑结构,输出功率达到了瓦级以上,但是腔长均在1 m以上,且腔体积较大。Aadhi等^[13]使用4个凹面镜的四镜环形腔实现了短腔长结构,进一步减小了激光腰斑,降低了激光输出阈值并提高了转换效率,但他们在该实验中使用的倍频晶体是走离效应较大的BiB₃O₆(BIBO)晶体,最终输出的倍频光功率最大值为770 mW。为了获得结构紧凑、转换效率高且输出波长覆盖近红外到中红外波段的激光光源,本团队设计了结构紧凑的四镜环形单共振光学参量振荡器(SRO),光学参量振荡晶体和倍频晶体分别是MgO:PPLN和周期极化磷酸氧铽(PPKTP)。最终,本团队实现了输出功率大于瓦级的覆盖近红外到中红外的高功率775 nm、1550 nm和3393 nm三波长激光输出。

2 光参量振荡器设计

相比于普通的双折射晶体,准相位匹配晶体可以利用其周期性分布结构有效补偿非线性频率变换过程中的相位失配,从而实现较高的光光转换效率和较高的激光输出功率。因此,本团队在实验中均使用周期极化晶体作为光学参量振荡晶体和倍频晶体。在1 μm激光泵浦产生1.5 μm激光的光学参量振荡器中,PPLN晶体因具有宽透明窗口、低吸收损耗和高非线性系数等优点而被广泛使用。但是,普通PPLN晶体的光折变效应比较明显,这会导致相位失配,严重时还会造成晶体损伤。在PPLN晶体中掺杂5%(质量分数)的MgO可以大幅降低晶体的光折变效应,进而提高晶体的损伤阈值。因此,本团队用MgO:PPLN晶体作为光学参量振荡晶体,其尺寸为1 mm×10 mm×40 mm,极化周期为30.49 μm。同时,为了实现1.5 μm激光的高效倍频,实验中用光折变效应不明显且非线性系数较大的PPKTP晶体作为倍频晶体,其尺寸为2 mm×2 mm×15 mm,极化周期为24.7 μm。

当1 μm激光注入到光学参量振荡器中产生1.5 μm和3.3 μm激光时,由三波耦合波方程可知,要想获得高效、高功率的单频连续波1.5 μm激光输出,光学参量振荡晶体MgO:PPLN处的腰斑半径是一个决定性参数。早在1968年Boyd等^[14]就引入了一个无量纲函数 h 来表示非线性频率变换过程的转换效率。函数 h 由双折射参量 B 以及聚焦因子 ξ 决定。同时,Boyd指出,对于不同的双折射参量 B ,总有一个最佳的聚焦因子 ξ 可以保证函数 h 的值为最大,此时,非线性频率变化过程的转换效率也最大。尤其是当非线性晶体为周期极化晶体时,双折射参量 B 为0,此时函数 h 的最大值可以达到1.06,对应的聚焦因子 ξ 为2.84。信号光的聚焦因子 ξ_s 和腰斑半径的关系可以

表示为

$$\xi_s = \frac{l}{b_s} = \frac{l\lambda_s}{2\pi n_s \omega_s^2}, \quad (1)$$

式中: l 为晶体长度; b_s 为信号光共焦参量; λ_s 为信号光波长; n_s 为晶体对信号光的折射率; ω_s 为信号光在晶体处的腰斑半径。根据式(1)中聚焦因子的选取可以得到此时光学参量振荡晶体MgO:PPLN处的腰斑半径为33.3 μm。为了实现泵浦光和信号光的高效匹配,进而获得高输出功率的1.5 μm和3.3 μm激光,泵浦光在MgO:PPLN晶体处的腰斑半径应为22.9 μm。如此小的泵浦光腰斑半径和振荡激光腰斑半径,会使光学参量振荡晶体MgO:PPLN出现严重的热透镜效应,甚至会引起晶体损伤,不利于1.5 μm和3.3 μm激光的产生。为了降低腰斑半径过小导致的光学参量振荡晶体MgO:PPLN的热效应并延长其使用寿命,在实际实验中,本团队采用聚焦因子 $\xi = 1$ 时对应的腰斑半径进行光学参量振荡器的设计和研究。这样,由式(1)以及光学参量振荡器的相关参数可知信号光在MgO:PPLN晶体处的腰斑半径为70 μm,此时,对应的泵浦光的腰斑半径为57.5 μm。

在保证光学参量振荡晶体处的腰斑尺寸的前提下,为了获得高效的单频775 nm激光输出,还需要通过设计合适的腔型结构来获得另一个较小的腰斑。同时为了使激光系统更加紧凑稳定,本团队在实验中采用了非平面镜的四镜环形谐振腔结构。要想获得稳定运转的内腔倍频光学参量振荡器,必须考虑光学参量振荡晶体的热透镜效应对光学参量振荡器的影响。在泵浦光泵浦MgO:PPLN晶体产生信号光和闲频光过程中,MgO:PPLN晶体对泵浦光、信号光和闲频光均会产生一定的吸收,因此晶体中的温度呈梯度分布,晶体会产生等效热透镜效应。根据文献[15-16],光学参量振荡晶体MgO:PPLN对泵浦光、信号光和闲频光的吸收系数 α 分别为0.25%、0.08%、35% cm⁻¹。非线性晶体的热透镜焦距可以表示为

$$\frac{1}{f} = \frac{\alpha(dn/dT)P_c}{\pi K_c} \int_{-l/2}^{l/2} \frac{dz}{\omega^2(z)}, \quad (2)$$

式中: f 为热透镜焦距; dn/dT 为晶体的热光系数; K_c 为晶体的热导率; l 为光学参量振荡晶体的长度; $\omega(z)$ 为 z 处的光斑半径; P_c 为腔内光功率。 P_c 与泵浦阈值 P_{th} 的计算公式^[17]分别为

$$P_c = 4 \frac{\lambda_p \beta g_1}{\lambda_s C_1 T} \left(1 - \frac{P_{th}}{P_p}\right), \quad (3)$$

$$P_{th} = \frac{(T + \epsilon) \left(1 + \frac{\omega_p^2}{\omega_s^2}\right) (k - 1) n_p n_s \lambda_i^2 \lambda_s c \epsilon_0}{32\pi^2 d^2 l \xi_s}. \quad (4)$$

式中: β 为腔内线性损耗,包括晶体表面镀膜的透射损耗和腔镜反射损耗; λ_p 、 λ_s 和 λ_i 分别为泵浦光、信号光和闲频光的波长; n_p 和 n_s 为晶体对泵浦光和信号光

的折射率; d 为晶体的有效非线性系数; c 为真空中的光速; ϵ_0 为真空介电常数; ϵ 为介电常数; P_p 为泵浦功率; T 为输出耦合镜对1550 nm激光的透射率; ω_p 为泵浦光在晶体处的腰斑半径; ω_s 为信号光在晶体处的腰斑半径; ξ_s 为信号光的聚焦因子; C_1 和 g_1 是与晶体和激光腰斑半径有关的常数。在不考虑相位失配时, C_1 和 g_1 可简化成

$$\begin{cases} C_1 = \frac{128\pi^2 d^2 l}{n_p n_s \lambda_p^2 \lambda_s c \epsilon_0} \\ g_1 = 3 \frac{(k-1)(1+2m)}{\xi_s (1+m)} \end{cases}, \quad (5)$$

式中: $k = \lambda_s / \lambda_p$; $m = \omega_p^2 / \omega_s^2$ 。

在输出耦合透镜透射率为1%的情况下,由式(2)可以得到泵浦光、信号光和闲频光功率与晶体热透镜焦距的关系。当注入泵浦功率为21 W时,由泵浦光引起的光学参量振荡晶体MgO:PPLN的热透镜焦距大约为400 mm,如图1(a)所示。此时,将输出耦合透镜的透射率 $T=1\%$ 代入式(3),可得腔内共振信号光功率 P_c 的大小为468 W,此时产生的闲频光功率约为2.56 W。尽管晶体对信号光的吸收较弱,但腔内功率较大,由信号光引起的热透镜焦距约为82.6 mm,如图1(b)所示。MgO:PPLN晶体对闲频光的吸收较强,但是产生的闲频光的功率较低,计算可得闲频光产

生的热透镜焦距约为400 mm,如图1(c)所示。图1(d)为三波长引起的光学参量振荡晶体总热透镜焦距随泵浦功率变化的曲线,可以看出光学参量振荡晶体MgO:PPLN的热透镜焦距主要是由晶体对腔内大功率信号光的吸收引起的。加入PPKTP晶体后的热透镜焦距可以采用相同的方法求得,在腔内信号光功率为468 W时加入倍频晶体。在考虑倍频晶体的非线性损耗后,计算得到腔内信号光功率为262 W。随后利用式(2)可以求得此时光学参量振荡晶体MgO:PPLN和倍频晶体PPKTP的热透镜焦距分别约为130 mm和181 mm。由于加入倍频晶体后,腔内部分振荡的信号光会转换成倍频激光输出,腔内振荡的信号光功率减小。经计算可知,在上述功率下,PPKTP晶体的热透镜焦距对谐振腔稳区和PPLN晶体处腰斑半径的影响不大,所以本文忽略了PPKTP晶体的热透镜效应。

最终在考虑MgO:PPLN晶体热透镜效应的基础上,利用ABCD矩阵计算谐振腔的参数,得到了四镜环形谐振腔内各处腰斑半径的变化图,如图2所示。从计算结果可以看出,在总腔长为406 mm的条件下,信号光在光学参量振荡晶体MgO:PPLN处的腰斑半径 ω_1 为70 μm ,在倍频晶体PPKTP处的腰斑半径 ω_2 为52 μm ,满足本实验需求。

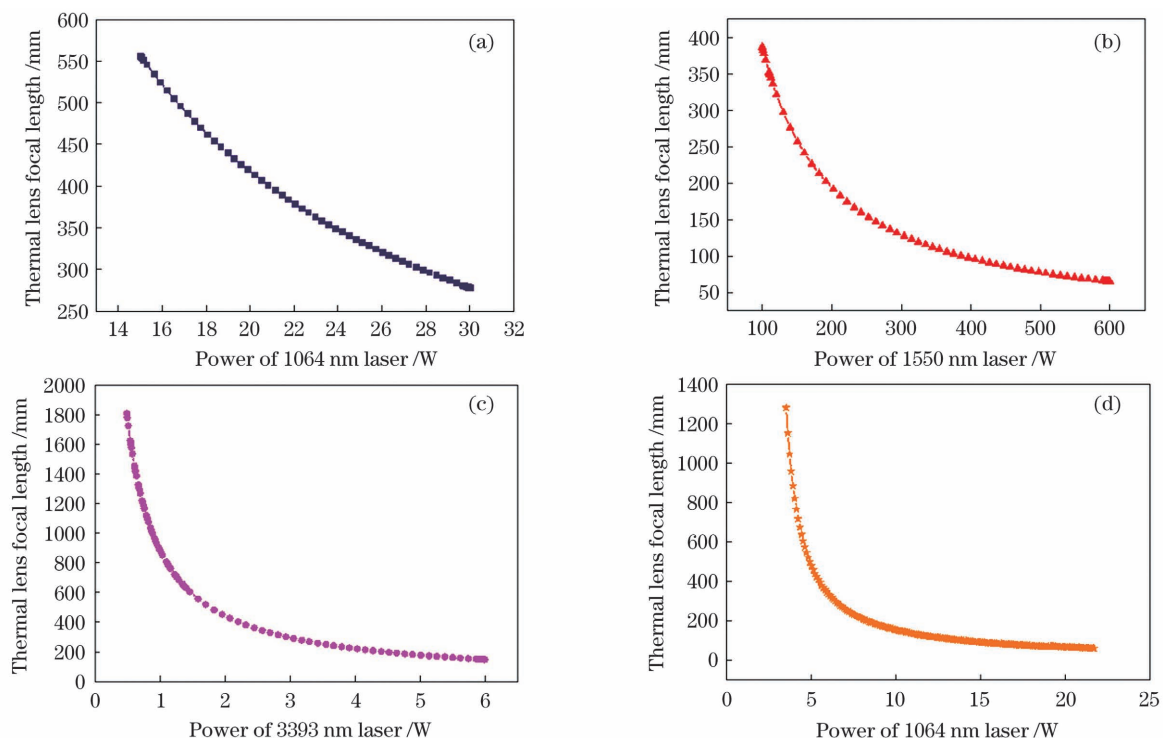


图1 估算的MgO:PPLN晶体的热透镜焦距。(a)泵浦光导致的热透镜焦距;(b)信号光导致的热透镜焦距;(c)闲频光导致的热透镜焦距;(d)MgO:PPLN晶体的总热透镜焦距

Fig. 1 Estimated thermal lens focal length of MgO:PPLN crystal. (a) Thermal lens focal length caused by pump laser; (b) thermal lens focal length caused by signal laser; (c) thermal lens focal length caused by idler laser; (d) whole thermal lens focal length of MgO:PPLN crystal

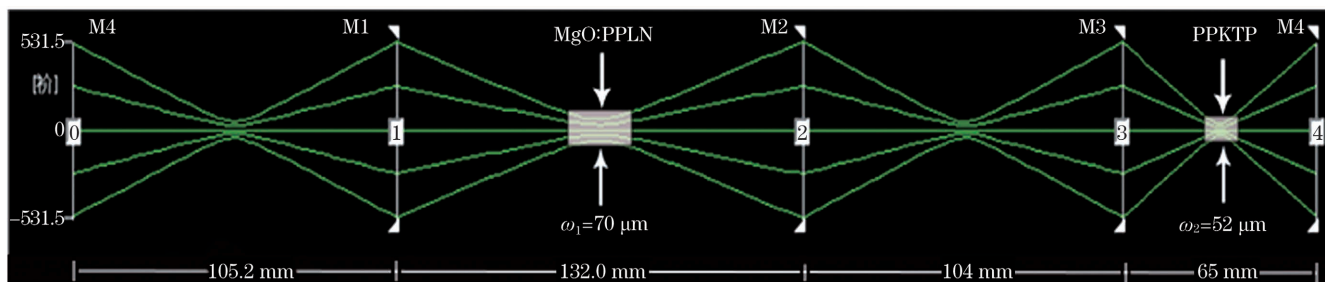


图2 谐振腔内腰斑的变化情况

Fig. 2 Waist variation in resonant cavity

3 实验装置

根据理论计算,本团队设计了如图3所示的四镜环形光学参量振荡激光器。泵浦源选用的是自主研发的全固态单频连续波1064 nm/532 nm双波长激光器^[18-19],其功率稳定性优于 $\pm 1\%$ (5 h),光束质量 M^2 优于1.2,单频1064 nm激光的偏振状态为水平偏振,偏振比高达100:1。首先采用双色分光镜(BS1)将双波长激光器的1064 nm激光和532 nm激光分开,单频532 nm激光被注入到功率计中,用于监视激光器的工作状态。从双色镜透射出的单频1064 nm激光首先被一个焦距为 $f_1=200$ mm的平凸透镜整形成一束近平行光。为了防止反射光对泵浦源的稳定运转产生不利影响,在单频1064 nm激光传输光路上放置了一个光隔离器(OI),OI前面的1/2波片(HWP1)用于校准入射到OI上的单频1064 nm激光的偏振方向。OI后面放置的另一个1/2波片(HWP2)用来校准进入光学参量振荡器中的单频1064 nm激光的偏振方向。为了实现泵浦光和光学参量振荡器精确模式的匹配,在光学参量振荡器前面放置了焦距为 $f_2=130$ mm的透镜,这样,单频1064 nm激光就会被聚焦成光斑半径为 $57.5 \mu\text{m}$ 的光束并入射到光学参量振荡晶体上。光学参量振荡器由4个非平面镜(M1、M2、M3和M4)组成,其中,M1是曲率半径为 $R=60$ mm的凹凸镜,M2是曲率半径为 $R=60$ mm的平

凹镜,M3、M4都是曲率半径为 $R=40$ mm的平凹镜。为了保证产生的 $1.5 \mu\text{m}$ 信号光在谐振腔内共振,泵浦光和产生的闲频光单次穿过,腔镜M1的凸面镀有1064 nm减反膜,凹面镀有1064 nm减反膜和1400~1700 nm高反膜;腔镜M2的凹面镀有1400~1700 nm高反膜和3000~4200 nm减反膜,平面镀有3000~4200 nm减反膜;腔镜M3镀有1400~1700 nm高反膜;输出耦合镜M4的凹面镀有1400~1700 nm部分透射率膜($T=1\%$)和730~850 nm减反膜,平面镀有1400~1700 nm和730~850 nm双减反膜。光学参量振荡晶体放置在腔镜M1和M2之间,倍频晶体放置在腔镜M3和M4之间。光学参量振荡晶体MgO:PPLN的尺寸为 $1 \text{ mm} \times 10 \text{ mm} \times 40 \text{ mm}$,MgO的掺杂浓度为5%(质量分数),极化周期为 $30.49 \mu\text{m}$ 。晶体侧面用铝箔包裹后安装在导热性能良好的紫铜炉中,紫铜炉和热沉之间放置一块半导体制冷片(TEC)用于热传导。热敏电阻放在紫铜炉靠近晶体的小孔内,用于实时探测紫铜炉乃至光学参量振荡晶体的工作温度。整个装置的温度由控温精度为 $0.01 \text{ }^\circ\text{C}$ 的YG-4S型高精度温控仪进行控制。倍频晶体PPKTP的尺寸为 $2 \text{ mm} \times 2 \text{ mm} \times 15 \text{ mm}$,极化周期为 $24.7 \mu\text{m}$,放置在同样的控温装置中进行实验。

单频1064 nm激光经过MgO:PPLN后产生信号光和闲频光,其中:闲频光从M2透射输出,可以用一个双色分光镜BS2将剩余的泵浦光和闲频光分开;信

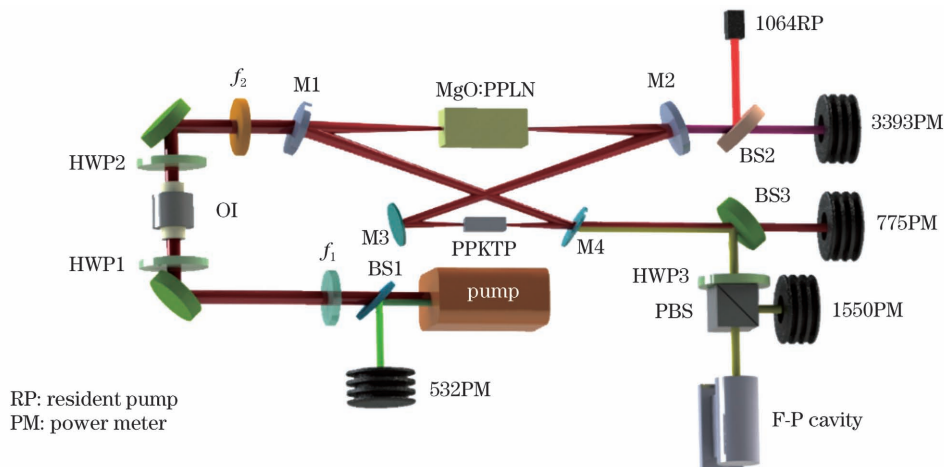


图3 实验装置图

Fig. 3 Diagram of experimental setup

号光在腔内形成稳定振荡后,一部分会与产生的倍频光一起从M4透射输出。输出的信号光和倍频光用一个1550 nm高反和775 nm高透的双色镜(BS3)分开,1550 nm光束进入一个由半波片(HWP3)和偏振分束棱镜(PBS)构成的功率分束组合,大部分输出激光进入功率计探测功率,小部分输出激光进入F-P干涉仪,用于监视输出激光的纵模模式。

4 实验结果及分析

通过扫描MgO:PPLN晶体的工作温度,可以实现信号光和闲频光的频率调谐。当MgO:PPLN晶体的工作温度为51℃时,信号光的输出波长为1550 nm,闲频光的输出波长为3393 nm,二者的输出功率随泵浦光功率的变化曲线如图4所示。由图4可以看出,当注入泵浦光功率为21 W时,获得了4.1 W的1550 nm信号光输出和2.1 W的3393 nm闲频光输出,光学参量振荡器的泵浦阈值为6 W,总的光学转换效率为30%。在光学参量振荡器稳定运转时,本团队用BP209-VIS光束质量分析仪测量了1550 nm信号光的光束质量,输出激光在X和Y方向上的质量因子分别为 $M_x^2 = 1.03$ 和 $M_y^2 = 1.05$,如图5所示。图5中的插图是单频1550 nm激光的光斑图,可以看出,获得的单频1550 nm信号光的强度分布基本上接近标准的高斯分布。同时,本团队还采用自零拍探测系统^[20]对获得的1550 nm信号光的强度噪声进行了测量。光束经过偏振分束棱镜分成两束进入两个光电探测器转化成电流信号后进行加/减法运算,其中加法运算后的电流代表强度噪声,减法运算后的电流代表对应的散粒噪声。光电流从直流信号(DC)端输出到示波器(OS),通过观察示波器电压的变化来保证两臂光功率完全相同;交流信号(AC)端的光电流输出到频谱仪(SA),通过频谱仪观测激光噪声谱线,频谱仪的分辨率带宽(RBW)和视频带宽(VBW)分别设置为30 kHz和30 Hz。最终得到的归一化强度噪声谱如图6所示,信号光在1.6 MHz处即达到散粒噪声基准(SNL)。

随后,本团队在M3、M4之间的腰斑处放入

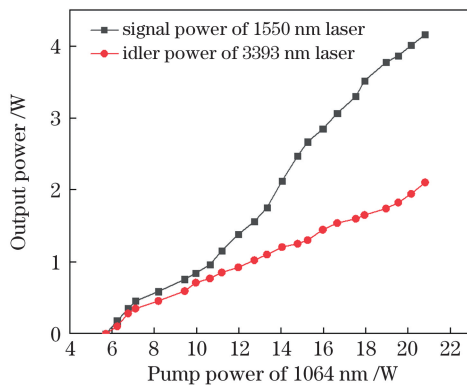


图4 信号光和闲频光输出功率随泵浦光功率的变化
Fig. 4 Output power of signal and idler lasers versus incident pump power

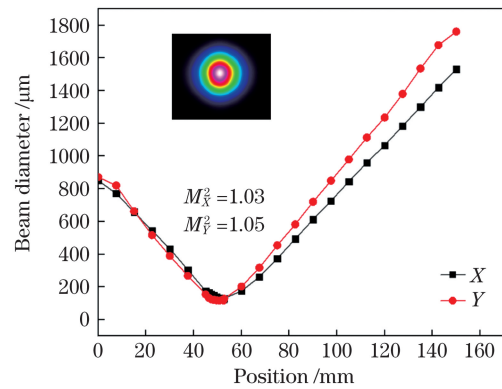


图5 1550 nm激光光束质量分析图

Fig. 5 Beam quality analysis of 1550 nm laser

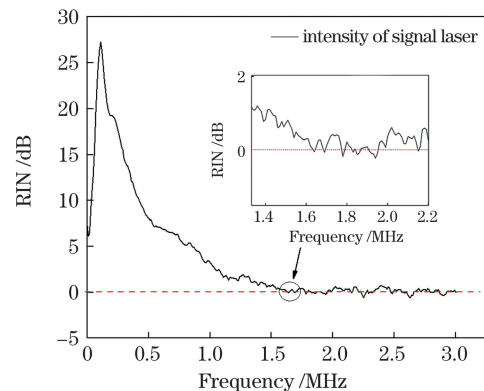


图6 未加倍频晶体时1550 nm激光的归一化强度噪声谱

Fig. 6 Normalized intensity noise (RIN) spectrum of 1550 nm laser without PPKTP

PPKTP晶体。由于PPKTP晶体的折射率较大($n_p = 1.81$),因此M3和M4之间的等效长度减小了6.71 mm(计算公式为 $l' - l'/n_p$,其中 l' 为PPKTP晶体的长度, $l' = 15$ mm)。等效腔长的变化会改变光学参量振荡晶体处的模式匹配。若要进一步获得高功率三波长激光输出,需要进一步优化M3和M4之间的腔长参数,实现最优模式匹配。在实现精确的模式匹配后,实现了稳定的三波长单频激光输出,此时信号光和倍频光输出功率随泵浦功率的变化如图7所示。输出信号光的激光泵浦阈值为8.3 W,在泵浦光功率上升过程中,当信号光输出功率为0.3 W时倍频光才开始输出;当泵浦功率大于16 W后,随着信号光输出功率的增大,倍频光的输出功率增加缓慢,倍频光的转换效率逐渐饱和。这主要是因为:1)信号光在腔内共振,腔内激光功率密度较高,PPKTP晶体对红外光的吸收以及外部控温系统引起的晶体温度梯度的分布,导致晶体折射率变化,从而使得谐振腔匹配模式发生变化,输出功率降低;2)随着腔内信号光功率密度的增大,PPKTP晶体内可能会产生高阶准相位匹配以及信号光高阶谐波产生等非线性效应,这些非线性效应进一步限制了倍频光的输出。当注入泵浦功率为21 W时,获得了2.1 W的信号光、1.1 W的倍频光以及1.7 W的闲频光输出,总的光光转换效率为23.3%。在此情况下,本团队测试了实验中获得三种波长激

光的功率稳定性,结果显示:在5 h内,信号光的功率稳定性(均方根,RMS)优于2.5%,倍频光的功率稳定性(RMS)优于1.6%,闲频光的功率稳定性(RMS)优于0.8%,如图8所示。利用F-P干涉仪监视光学参量振荡的单频特性,得到的结果如图9所示。可以看到激光器在该功率下可以实现稳定的单纵模运转。在此状态下,本团队利用光束质量分析仪测量了所获得的倍频光的光束质量,测量结果如图10所示,可以

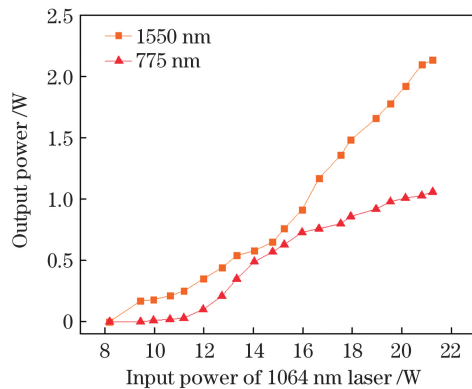


图7 加入 PPKTP 后 1550 nm/775 nm 激光输出功率随泵浦功率的变化

Fig. 7 Output power of 1550 nm/775 nm laser versus incident pump power after adding PPKTP

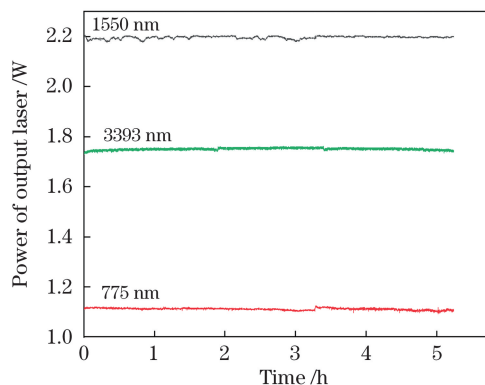


图8 信号光(1550 nm)、闲频光(3393 nm)和倍频光(775 nm)5 h 内的功率稳定性

Fig. 8 Power stability of signal laser (1550 nm), idler laser (3393 nm), and frequency-doubled laser (775 nm) within 5 h

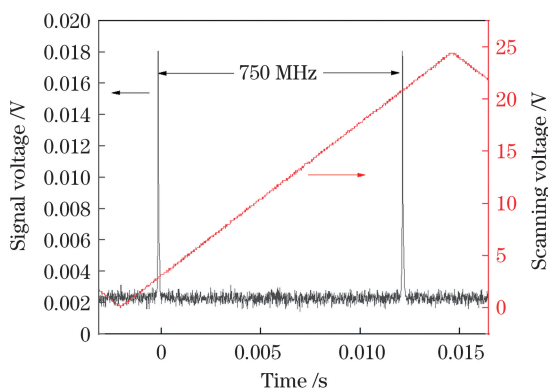


图9 测量的 1550 nm 激光的单频特性

Fig. 9 Single frequency characteristics of 1550 nm laser measured in experiment

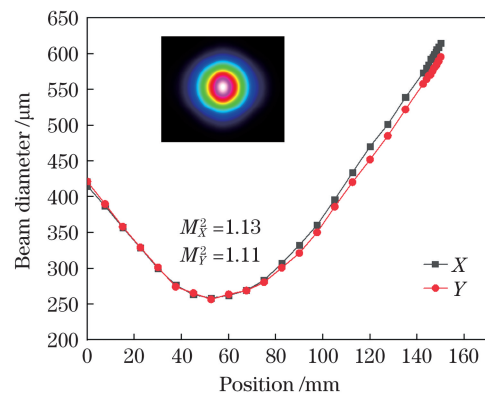


图10 775 nm 激光的光束质量分析

Fig. 10 Beam quality analysis of 775 nm laser

看出,775 nm 倍频光在 X 和 Y 方向上的质量因子分别为 $M_x^2 = 1.13$ 和 $M_y^2 = 1.11$ 。

5 结 论

本团队采用结构紧凑的四镜环形单共振光学参量振荡器以及周期极化晶体实现了瓦级从近红外到中红外的单频连续波激光输出。首先通过分析 OPO 的聚焦因子以及非线性晶体的热透镜效应对激光器稳区、腰斑半径的影响,设计了结构紧凑的四镜环形单共振光学参量振荡器,该结构不仅满足了光学参量振荡过程的要求,还可以实现高效稳定的腔内倍频;然后在谐振腔的两个腰斑处分别放置光学参量振荡晶体 MgO:PPLN 和倍频晶体 PPKTP,实现了从近红外到中红外的倍频光、信号光和闲频光三波长高功率单频连续波激光输出,信号光、倍频光及闲频光的最大输出功率分别达到了 2.1、1.1、1.7 W,总的光光转换效率达 23.3%,光束质量均优于 1.13,三波长功率稳定性(RMS)均优于 2.5%。该单频连续波激光器可广泛应用于量子光学以及量子技术研究中,其同时产生的信号光和倍频光可以分别作为种子光和泵浦光同时注入到新的 OPO 中直接产生 1550 nm 压缩态光场,为进一步制备多组分纠缠非经典光场奠定了基础。

参 考 文 献

- [1] 郭磊,陈怀熹,张新彬,等. 基于 MgO:PPLN 啁啾结构和频的宽谱黄-橙激光输出[J]. 激光与光电子学进展, 2020, 57(9): 091901.
Guo L, Chen H X, Zhang X B, et al. Broadband yellow-orange laser output based on chirp structure MgO:PPLN sum-frequency[J]. Laser & Optoelectronics Progress, 2020, 57(9): 091901.
- [2] 王庆,漆磊,王润雨,等. 飞秒激光脉内自差频产生中红外激光研究进展[J]. 激光与光电子学进展, 2021, 58(17): 1700001.
Wang Q, Qi L, Wang R Y, et al. Research progress of mid infrared laser via intra-pulse difference frequency generation of femtosecond laser[J]. Laser & Optoelectronics Progress, 2021, 58(17): 1700001.
- [3] Bekman H H P T, van den Heuvel J C, van Putten F J M, et al. Development of a mid-infrared laser for study of infrared countermeasures techniques[J]. Proceedings of SPIE, 2004, 5615: 27-38.
- [4] Nelson D D, Shorter J H, McManus J B, et al. Sub-part-per-

- billion detection of nitric oxide in air using a thermoelectrically cooled mid-infrared quantum cascade laser spectrometer [J]. *Applied Physics B*, 2002, 75(2/3): 343-350.
- [6] 姚子健, 李渊曠, 宋政, 等. 基于全固态单向行波环形腔的连续波单频 1.5 μm 激光器[J]. *中国激光*, 2021, 48(5): 0501010. Yao Z J, Li Y J, Song Z, et al. Continuous-wave single-frequency 1.5 μm laser based on all-solid-state unidirectional traveling-wave ring cavity[J]. *Chinese Journal of Lasers*, 2021, 48(5): 0501010.
- [7] 邵朝阳, 侯飞雁, 王盟盟, 等. 光纤激光经过模清洁剂后的强度噪声分析[J]. *物理学报*, 2014, 63(19): 194203. Tai Z Y, Hou F Y, Wang M M, et al. Intensity noise analysis of a fibre laser after passing through an optical mode cleaner[J]. *Acta Physica Sinica*, 2014, 63(19): 194203.
- [7] 王倩倩, 冯晋霞, 姜振宇, 等. 利用马赫-曾德尔干涉仪改善光纤激光器输出激光性能的研究[J]. *量子光学学报*, 2020, 26(1): 71-76. Wang Q Q, Feng J X, Jiang Z Y, et al. Investigation on improving the output performance of fiber laser using Mach Zehnder interferometer[J]. *Journal of Quantum Optics*, 2020, 26(1): 71-76.
- [8] 王菲菲, 聂鸿坤, 刘俊亭, 等. 小型化宽调谐 MgO:PPLN 中红外纳秒光参量振荡器[J]. *中国激光*, 2021, 48(5): 0501015. Wang F F, Nie H K, Liu J T, et al. Miniaturized widely tunable MgO:PPLN nanosecond optical parametric oscillator [J]. *Chinese Journal of Lasers*, 2021, 48(5): 0501015.
- [9] 张兴宝, 王月珠, 姚宝权, 等. 基于 PPLN 的中红外 CW QPM-OPO 技术发展综述[J]. *激光杂志*, 2005, 26(6): 7-9. Zhang X B, Wang Y Z, Yao B Q, et al. Development of mid-infrared CW QPM-OPO based on PPLN [J]. *Laser Journal*, 2005, 26(6): 7-9.
- [10] Mehmet M, Ast S, Eberle T, et al. Squeezed light at 1550 nm with a quantum noise reduction of 12.3 dB[J]. *Optics Express*, 2011, 19(25): 25763-25772.
- [11] Shukla M K, Maji P S, Das R. Yb-fiber laser pumped high-power, broadly tunable, single-frequency red source based on a singly resonant optical parametric oscillator[J]. *Optics Letters*, 2016, 41(13): 3033-3036.
- [12] Devi K, Kumar S C, Ebrahim-Zadeh M. High-power, continuous-wave, single-frequency, all-periodically-poled, near-infrared source[J]. *Optics Letters*, 2012, 37(24): 5049-5051.
- [13] Aadhi A, Chaitanya N A, Singh R P, et al. High-power, continuous-wave, solid-state, single-frequency, tunable source for the ultraviolet[J]. *Optics Letters*, 2014, 39(12): 3410-3413.
- [14] Boyd G D, Kleinman D A. Parametric interaction of focused Gaussian light beams[J]. *Journal of Applied Physics*, 1968, 39(8): 3597-3639.
- [15] Lowenthal D D. CW periodically poled LiNbO₃ optical parametric oscillator model with strong idler absorption [J]. *IEEE Journal of Quantum Electronics*, 1998, 34(8): 1356-1366.
- [16] Vainio M, Peltola J, Persijn S, et al. Thermal effects in singly resonant continuous-wave optical parametric oscillators [J]. *Applied Physics B*, 2008, 94(3): 411-427.
- [17] Guha S. Focusing dependence of the efficiency of a singly resonant optical parametric oscillator [J]. *Applied Physics B*, 1998, 66(6): 663-675.
- [18] Guo Y R, Lu H D, Xu M Z, et al. Investigation about the influence of longitudinal-mode structure of the laser on the relative intensity noise properties[J]. *Optics Express*, 2018, 26(16): 21108-21118.
- [19] Lu H D, Su J, Zheng Y H, et al. Physical conditions of single-longitudinal-mode operation for high-power all-solid-state lasers [J]. *Optics Letters*, 2014, 39(5): 1117-1120.
- [20] Guo Y R, Peng W N, Su J, et al. Influence of the pump scheme on the output power and the intensity noise of a single-frequency continuous-wave laser[J]. *Optics Express*, 2020, 28(4): 5866-5874.

Experimental Study of Near-Infrared to Mid-Infrared Laser Output Based on Single Resonant Optical Parametric Oscillator

Wang Hailong¹, Yang Huiqi¹, Su Jing^{1,2}, Lu Huadong^{1,2*}

¹ State Key Laboratory of Quantum Optics and Quantum Optics Devices, Institute of Opto-Electronics, Shanxi University, Taiyuan 030006, Shanxi, China;

² Collaborative Innovation Center of Extreme Optics, Shanxi University, Taiyuan 030006, Shanxi, China

Abstract

Objective Due to its small construction, low-intensity noise, and narrow linewidth, all-solid-state continuous-wave (CW) single-frequency lasers have been widely employed in scientific research, military, and medical applications. The emission wavelengths of lasers can be confined to many particular ranges due to the constraints of the fluorescence spectra of laser crystals, which cannot match the demands of rapidly increasing scientific research. As an effective laser wavelength conversion technology, the nonlinear frequency conversion process including optical parametric oscillation (OPO), sum frequency (SF), different frequency (DF), etc., provides multi-watt CW output powers in the deep-ultraviolet (DUV) to mid-infrared and further expands the applied field of lasers. The single-frequency 1550 nm laser is frequently utilized in the formation of quantum squeezed and entangled states because its wavelength matches the low dispersion and low loss window of fibers, allowing for long-distance and steady laser transmission through the fiber. At present, there are several methods to generate a 1550 nm laser. Firstly, the 1550 nm laser is produced by a laser crystal co-doped with ytterbium-erbium (Yb³⁺, Er³⁺) directly pumped by a 976 nm semiconductor laser. The low cost, small construction, and ease of downsizing draw a lot of interest, however, the gain crystal's intrinsic excited state absorption restricts the laser output power. Secondly, the 1550 nm laser is also produced by an erbium (Er³⁺)-doped fiber laser. The erbium-doped fiber laser's waveguide structure is advantageous for achieving high-power output, although the output laser's noise is rather high. In comparison to the previous approaches, the OPO process combines the benefits of low

noise, small line width, and high stability to make the single-frequency 1550 nm laser the ideal contender. Especially, when we would like to generate the 1550 nm squeezed and entangled states, it is needed to use 775 nm and 1550 nm lasers as the pump and signal lasers of the optical parametric amplifier (OPA), respectively. As a result, an intra-cavity frequency-doubled (FD) singly resonant optical parametric oscillator (SRO) made of four mirrors is created and reported in this research, with simultaneous watt-level CW single-frequency lasers at 775 nm, 1550 nm, and 3393 nm.

Methods In the experiment, to achieve high power signal laser and its frequency-doubled laser, it is important to acquire two focus waists in the cavity. The thermal lens effect of the MgO:PPLN crystal induced by the pump, signal, and idler lasers was initially estimated for this purpose. The thermal lens effect of MgO:PPLN is mostly due to its absorption of high-power intra-cavity signal lasers, according to theoretical simulations. On this basis, a ring resonator including two small waists was designed and built, which consists of four concave mirrors (radius of curvature of mirrors M1 and M2 is 60 mm and that of mirrors M3 and M3 is 40 mm), and whose whole length was optimized to 406 mm. The waist radii of the signal lasers at the OPO and second harmonic generation (SHG) crystals were 70 μm and 52 μm , respectively, in this scenario. To ensure a singly resonant optical parametric oscillator for the signal and single-pass transmission for the pump and idler lasers, the input coupler M1 was coated with high reflection (HR, reflectivity $R > 99.8\%$) film for the signal laser across 1400–1700 nm and high transmitting (HT, transmittivity $T > 97\%$) film for the pump 1064 nm laser. Mirror M2 was coated with HR ($R > 99.8\%$) film for the signal laser and HT ($T > 95\%$) film for the idler laser (3000–4200 nm). Mirror M3 was coated with HR ($R > 99.8\%$) film for the signal laser. Mirror M4 was coated with 1% transmission film for signal laser and HT ($T > 95\%$) film for frequency-doubled laser across 730–850 nm. The pump source was a handmade all-solid-state CW single-frequency 1064 nm laser with good performance. A coupling system consisting of an optical isolator (OI), two half wave-plates (HWP), and two lenses oriented and focused the output laser beam on the OPO. A 40 mm long 5% MgO-doped periodically poled PPLN crystal (polarization cycle $\Lambda = 30.49 \mu\text{m}$) was used as the OPO crystal owing to its wide transparent window and low absorption loss, which was placed at the focus point between the mirrors M1 and M2 to generate the high efficiency and high-power signal and idler lasers. For the intra-cavity SHG crystal, a PPKTP crystal ($\Lambda = 24.7 \mu\text{m}$) with the size of 2 mm \times 2 mm \times 15 mm was used and placed at the other waist between mirrors M3 and M4. For signal and frequency-doubled lasers, both sides of the crystals were covered with antireflection coatings. Both crystals were kept in separate ovens, each controlled by a 0.01 $^{\circ}\text{C}$ high precision temperature controller. The high-quality watts single-frequency infrared to mid-infrared laser output was generated by controlling the temperature of MgO:PPLN and PPKTP to 51 $^{\circ}\text{C}$ and 40.2 $^{\circ}\text{C}$, respectively.

Results and Discussions Using a small double waists single resonance oscillation and periodically polarized crystal, a single-frequency CW three-wavelength laser output from the near-infrared to the mid-infrared at the watt level was obtained. Figure 1 depicts the effect of the pump, signal, and idler lasers on the thermal lens focal length of MgO:PPLN crystal. It is shown that the effect of signal laser on the thermal lens focal length of MgO:PPLN crystal is much larger than that of idle and pump lasers. A compact four-mirror ring SRO was designed as Fig. 2. We obtained 4.1 W of 1550 nm signal laser output power and 2.1 W of 3393 nm idler laser output power when the input pump power was 21 W (Fig. 4), the quantity factor M^2 of 1550 nm laser was better than 1.05 (Fig. 5). The measured output power of signal and SHG lasers vs the input pump power is shown in Fig. 7. The pump threshold was discovered to be 8.3 W. When the incident pump power was raised to 16 W, more nonlinear effects appeared in the crystal as the signal laser power in the cavity rose, resulting in a reduction in FD conversion efficiency. When the pump power was increased to 21 W, the laser was operating stable and the output powers of 1550, 775, and 3393 nm lasers were 2.1, 1.1, and 1.7 W, respectively. The root-mean-square (RMS) variations of the output power during 5 h are less than 2.5% for the 1550 nm laser, 0.8% for the 3393 nm laser, and 1.6% for the 775 nm laser, respectively (Fig. 8). The overall efficiency of light-to-light conversion was 23.3%. The 775 nm lasers' measured beam quality was better than 1.13. (Fig. 10). The output laser operates in a single longitudinal mode.

Conclusions The experimental findings of the creation of near-infrared to mid-infrared lasers employing an SRO made up of four-mirror ring resonators and period poled crystals were described in this study. To begin, we looked at OPO's focusing characteristics as well as the impact of the nonlinear crystal's thermal lens effect on the laser stable area and waist size. On this basis, a four-mirror ring resonator structure with double small waists was designed. Then, as the OPO and frequency-doubling crystals, a MgO:PPLN and a PPKTP were used to create the signal and frequency-doubled lasers, as well as the idler laser. When the pump power was 21 W, the output power of the 1550 nm signal laser could reach up to 2.1 W. The output powers of the 775 nm frequency-doubled laser and 3393 nm idler lasers were 1.1 W and 1.7 W, respectively, at the same time. The pump threshold was 8.3 W, the overall light-to-light conversion efficiency was 23.3%, and the beam quality was greater than 1.05 and 1.13 at 1550 and 775 nm, respectively. The RMS fluctuations of the power during 5 h were less than 2.5% of 1550 nm, 0.8% of 3393 nm, and 1.6% of 775 nm. The 775 nm and

1550 nm lasers created can be utilized as the pump and seed lasers of OPO and OPA, respectively, in quantum experiments to generate a 1550 nm compressed light field. It gives a trustworthy assurance for the development of a multi-component quantum light source, and it is viewed as a novel technological technique of attaining compact quantum squeezed state laser source manufacture.

Key words lasers; singly resonant optical parametric oscillator; frequency-doubling; four-mirror ring cavities; single-frequency; thermal lens effect